

# Computing Shor's algorithmic steps with classical light beams

Wei Wang,<sup>1</sup> Ziyang You,<sup>1</sup> Shuangpeng Wang,<sup>1</sup> Zikang Tang,<sup>1</sup> and Hou Ian<sup>1,\*</sup>

<sup>1</sup>*Institute of Applied Physics and Materials Engineering,  
University of Macau, Macau S.A.R., China*

When considered as orthogonal bases in distinct vector spaces, the unit vectors of polarization directions and the Laguerre-Gaussian modes of polarization amplitude are inseparable, constituting a so-called classical entangled light beam. We apply this classical entanglement to demonstrate theoretically the execution of Shor's factoring algorithm on a classical light beam. The demonstration comprises light-path designs for the key algorithmic steps of modular exponentiation and Fourier transform on the target integer 15. The computed multiplicative order that eventually leads to the integer factors is identified through a four-hole diffraction interference from sources obtained from the entangled beam profile. We show that the fringe patterns resulted from the interference are uniquely mapped to the sought-after order, thereby emulating the factoring process originally rooted in the quantum regime.

## I. INTRODUCTION

Non-zero correlation between space-like events was initially debated in the famous Einstein-Podolsky-Rosen thought experiment [1]. This contemplated correlation was later quantified by Bell's inequality [2] and CHSH inequality [3], which subsequently give rise to the concept of quantum entanglement [4]. Violating the law of locality, entanglement has long been thought of as a unique feature only for systems operating in the quantum regime [5]. But recent investigations have revealed that entanglement to some partial extent can be emulated in classical systems [6–8]. In particular, the classical entanglement between the polarization direction and the polarization amplitude is experimentally verified [9]; so is that between the polarization and the Orbital Angular Momentum (OAM) in a Laguerre-Gaussian (LG) beam [10].

Entanglement plays a key role in implementing quantum algorithms. The celebrated Shor's algorithm relies on the entanglement of two quantum states, guised as two computational registers, to speed up the finding of the correct factor of a large integer [11]. The two registers can be physically realized by superconducting qubits [13], nuclear spins [14], or optical photons [15–17]. Comparing to quantum entanglement exemplified in the these quantum systems, classical entanglement can obtain a similar correlation level while having additional merits of coherence, generation, and detection [18, 19]. Therefore, classical entanglement has potentials in some applications intended for quantum systems, such as quantum communication and computation [20–22]. Several quantum algorithms, including Deutsch algorithm [23], quantum walk [24], and quantum Fourier transform (QFT) [10], have been implemented with classical entanglement. Nonetheless, the realization of Shor's algorithm in classical optics is less explored.

In this work, we demonstrate a fully compiled version of Shor's factoring algorithm for  $N = 15$  utilizing just classical LG beams and common optical elements. In particular, the OAM degree of freedom of LG beams is made to represent the computational basis for the control register in Shor's algorithm. Meanwhile, the polarization directions perform the role as the work register, storing values for modular exponentiation and discrete Fourier transform, two key steps of the Shor's algorithm. The two steps are implemented by sending the beams into a series of optical elements, during which the two degrees of freedom described are entangled in the beam profiles. Since classical entanglement can be detected in the interference fringes of a light beam [25], the computational information encoded in the LG beam profiles are eventually determined from a four-hole interference at the end of the light path. We show the distinguishability of the resulting fringes for distinct

---

\* houian@um.edu.mo

orders and demonstrate the particular order elicited from the fringe pattern for the case of  $N = 15$ . This work therefore presents evidence that, theoretically speaking, quantum algorithms are not necessarily exclusive to classical systems and that the so-called quantum and classical regimes are not as mutually exclusive as usually thought.

In the following, we present the algorithmic steps based on LG beams in Sec. II. Proposals for optical path implementations are explained in Sec. III and the detection methods discussed in Sec. IV. Conclusions and discussions regarding the advantages and disadvantages of the current approach are given in Sec. V.

## II. CLASSICAL ENTANGLEMENT AND SHOR'S ALGORITHM

Classical entanglement refers to non-separable correlations among the degrees of freedom in classical optics. For instance, the two orthogonal polarization directions ( $\mathbf{e}_x$  and  $\mathbf{e}_y$ ) and their respective field amplitudes ( $E_x$  and  $E_y$ ) can be taken as an entangled pair in the polarized optical field  $\mathbf{E} = E_x \mathbf{e}_x + E_y \mathbf{e}_y$ . Allowing the field amplitudes to vary spatially beyond those depicted by plane waves, one arrives at linearly polarized LG beams

$$\mathbf{E} = u_{p,l} \mathbf{H} + u_{p,-l} \mathbf{V}, \quad (1)$$

where  $\mathbf{H}$  and  $\mathbf{V}$  denote the unit vectors for respectively horizontal and vertical polarization directions while

$$u_{p,l}(r, \varphi, z) = \frac{C(r\sqrt{2}/w_z)^{|l|}}{\sqrt{1 + z^2/z_R^2}} e^{-r^2/w_z^2} L_p^{|l|} \left( \frac{2r^2}{w_z^2} \right) \times e^{-il\varphi} \exp i \left\{ \frac{kr^2 z}{2(z^2 + z_R^2)} + (2p + |l| + 1) \tan^{-1} \frac{z}{z_R} \right\} \quad (2)$$

indicate the distribution function for the OAM-mode amplitudes in cylindrical coordinates [26] with  $z$  being the propagation direction. In the equation,  $C$  is a normalized constant,  $z_R$  the Rayleigh range,  $w_z$  the beam waist, and  $L_p^{|l|}$  the associated Laguerre polynomial. It is worth noting that the function has an azimuthal angular dependence of  $\exp(-il\varphi)$ , where  $l$  is the topological charge determining the angular momentum ( $l\hbar$  per photon) and the chirality of helical phase fronts (sign of  $l$ ).

The set of OAM-modes specified by the integer  $l$  forms an orthonormal set of basis functions for a complete Hilbert space, i.e. the inner product  $(u_{p,l}, u_{p,l'}) = \delta_{l,l'}$ . We make use of this property to encode the computational bases needed by Shor's algorithm in in the modes  $u_{p,l}$ , viz. letting  $|l\rangle = u_{p,l}$  in the bra-ket notation.

Shor's algorithm calls for the use of two computational registers, a control register and a work register, whose joint state is separable, i.e.  $|\psi_C\rangle \otimes |\psi_W\rangle$ , after initialization. The first algorithmic step [12] thereafter is the formation of the entangled state

$$\frac{1}{\sqrt{2^n}} \sum_{x=0}^{2^n-1} |x\rangle |a^x \pmod N\rangle \quad (3)$$

amongst the two registers, where the work register encodes the results of modular exponentiation function (MEF) according to the exponent  $x$  given in the control register and the modulus  $N$ . The integer  $N$  is the target integer to be factored and the base  $a < N$  is a pre-selected number coprime with  $N$ , i.e.  $\gcd(a, N) = 1$ . Number-theoretically speaking, factorizing  $N$  corresponds to finding an  $x$  value such that it becomes the multiplicative order of the MEF. The candidate of this order  $x$  lies within the range  $\{0, 1, \dots, 2^n - 1\}$ , hence the range of the summation, where  $n$  denotes the number of qubits necessary for constructing each register and is determined by  $N$ , i.e.  $2^n \approx \sqrt{N}$ . As an illustrating

example, here and below we consider the case  $N = 15$ , for which  $n = 2$  and  $a = 11$  are chosen. In other words,  $x \in \{0, 1, 2, 3\}$  while the exponentiation assumes two possible values, 1 and 11.

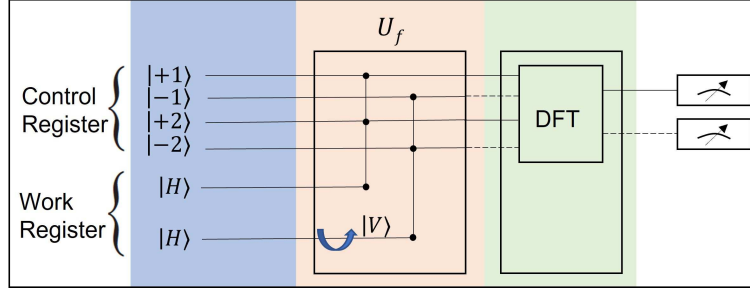


Figure 1. Circuit flow diagram for implementing Shor's algorithm with  $N = 15$  and  $a = 11$ . The blue, pink, and green parts indicate the stages for initialization, modular exponentiation, and discrete Fourier transform, respectively. The blue arrow in MEF in this part refers to the polarization flip. The modular exponentiation is implemented across the control and the work registers by a unitary transform  $U_f$ , before which one eigenstate of the work register is flipped (shown as the blue arrow) and after which the eigenstates across the two registers are distinctly entangled (shown by the black nodes). The two entangled states associated with  $|H\rangle$  and  $|V\rangle$  directions are separately passed on to the Fourier transform stage, respectively indicated by the solid and the dashed lines.

To establish the state of Eq. (3) in a classical beam of light for  $N = 15$ , we store control register information  $\psi_C \in \{0, 1, 2, 3\}$  into the OAM-modes with  $l = \{+1, -1, +2, -2\}$  of an LG beam and work register information  $\psi_W \in \{1, 11\}$  into the polarization directions  $\mathbf{H}$  and  $\mathbf{V}$  of that beam. To comply with the standard quantum bra-ket notation, we write the initial input state as

$$|\psi_{\text{in}}\rangle = (|+1\rangle + |-1\rangle + |+2\rangle + |-2\rangle) |H\rangle, \quad (4)$$

where the normalization constant is omitted to simplify the expression. Then, all algorithmic steps involved for computing the multiplicative order described by the originally quantum algorithm can be realized on Eq. (4) using just classical light path manipulations. Figure 1 shows the partitioning of the four major steps of Shor's algorithm: (i) preparing the initial state; (ii) performing modular exponentiation (MEF); (iii) performing quantum or discrete Fourier transform (DFT); and (iv) executing read out.

Before describing the detailed setup of an integrated light path for carrying out the forementioned four steps, we examine from a formal perspective how Eq. (4) changes in each stage to demonstrate that the final state of the LG beam contains computationally significant information. First, the MEF  $a^x \bmod N$  should set work register to 1 ( $|\psi_W\rangle = |H\rangle$ ) that associates with either the case  $x = 0$  or  $x = 2$ , i.e.  $|\psi_C\rangle = |+1\rangle$  or  $|+2\rangle$ , at the control register; complementarily, the work register stores 11 ( $|\psi_W\rangle = |V\rangle$ ) for  $x = 1$  or  $x = 3$  at the control register, i.e.  $|\psi_C\rangle = |-1\rangle$  or  $|-2\rangle$ . The entangled state after the MEF should read

$$|\psi_{\text{MEF}}\rangle = |+1, H\rangle + |-1, V\rangle + |+2, H\rangle + |-2, V\rangle, \quad (5)$$

where the necessary information for eliciting the correct multiplicative order is contained.

The next step in Shor's original routine involves a projective readout on Eq. (5) that collapses the work register into a definite  $|H\rangle$  or  $|V\rangle$  state, leaving the control register retain an eigenstate superposition. Note that the MEF entanglement guarantees that either way of the collapse will impose the same multiplicative order in the superposition. In our illustrated example, collapsing  $|\psi_W\rangle$  into either  $|H\rangle$  or  $|V\rangle$  will retain identically two eigenstates in  $|\psi_C\rangle$ ; whether either  $|+1\rangle + |+2\rangle$  or  $|-1\rangle + |-2\rangle$  points to the same order 2 (i.e.  $11^2 \bmod 15 = 1$ ). In contrast, deprived of the unique property of quantum collapse,

classical beams can substitute this step by simply splitting the mixed beam through a polarizing beam splitter (PBS). That is, the PBS would split out two equally significant beams

$$\begin{aligned} |\psi_H\rangle &= | +1, H\rangle + | +2, H\rangle, \\ |\psi_V\rangle &= | -1, V\rangle + | -2, V\rangle, \end{aligned} \quad (6)$$

on either of which the subsequent algorithmic steps can operate to achieve integer factoring of 15.

One of the polarized beam in Eq. (6) then undergoes the discrete Fourier transform (DFT) (the third major key illustrated in Fig. (1)) expressed as

$$|x\rangle \rightarrow \frac{1}{\sqrt{2^n}} \sum_{j=0}^{2^n-1} e^{i2\pi jx/2^n} |j\rangle. \quad (7)$$

Each state  $|x\rangle$  is transformed to a set of new orthogonal bases  $|j\rangle$  ( $j \in \{0, 1, \dots, 2^n - 1\}$ ) with a specific distribution of phases determined by the value of  $x$  in  $2^n$  dimensions ( $n = 2$  in this example). For typical quantum optical [16, 17] or superconducting circuit [13] implementations, Hadamard gates or control phase gates are consecutively applied to individual qubits to realize the Fourier transform, making the transform of Eq. (7) essentially an  $n$ -step one-qubit operation. The OAM space of the LG beam considered here need not be decomposed into 2-level spaces, so the phases can be imposed concurrently on the OAM modes  $|l\rangle$ , i.e. the DFT transform bases  $|j\rangle$ , once they are separated. In the illustrated example, since  $|j\rangle$  ranges over  $|+1\rangle$ ,  $|-1\rangle$ ,  $|+2\rangle$  and  $|-2\rangle$ , the intermediate state resulted from  $|l = -1\rangle$  for example becomes

$$\left| \psi_{\text{int}}^{(-1)} \right\rangle = | +1\rangle + i | -1\rangle - | +2\rangle - i | -2\rangle. \quad (8)$$

The phases  $\{0, \pi/2, \pi, 3\pi/2\}$  imposed can be realized by spiral phase plates (SPP) and phase-only spatial light modulators (SLM). While the former performs the function of converting OAM modes, e.g. from  $|+1\rangle$  to  $|+2\rangle$ , the latter introduces an arbitrary phase to a specific mode. Combining the two allows one to generate  $i|+1\rangle$  from  $|-1\rangle$  through the addition of a  $\pi/2$  phase.

To complete the DFT transform, each state that underwent Eq. (7) should be combined through addition, i.e. to arrive at

$$|\psi_{\text{DFT}}\rangle = \left| \psi_{\text{int}}^{(\pm 1)} \right\rangle + \left| \psi_{\text{int}}^{(\pm 2)} \right\rangle, \quad (9)$$

where the sign depends on which beams we choose from Eq. (6). The choice of the sign would lead the control register to retain either the superposition  $|+1\rangle + |+2\rangle$  or  $|+1\rangle - |+2\rangle$ . The phase difference between the two basis vectors does not affect the computation significance. Either state contains the OAM modes  $l = +1$  and  $l = +2$ , which translate into the computational values 0 and 2, respectively, according to the algorithmic premise we have assumed. Since only non-zero value is acceptable, one is left with  $x = 2$  from which the multiplicative order  $r = 2^n/x$  can be obtained. Then, the integer factors  $11^{r/2} \pm 1 = 3$  or  $5$  become apparent. The last two conversion steps are not computationally complex and thus not necessarily executed in the light paths.

### III. OPTICAL PATHS FOR ALGORITHMIC STEPS

The two major algorithmic steps according to Fig. 1 and the discussion in the last section are: (i) modular exponentiation function (MEF) and (ii) discrete Fourier transform (DFT). Below we examine the details of the experimental setup that can accomplish these two steps.

## 1. Modular Exponentiation

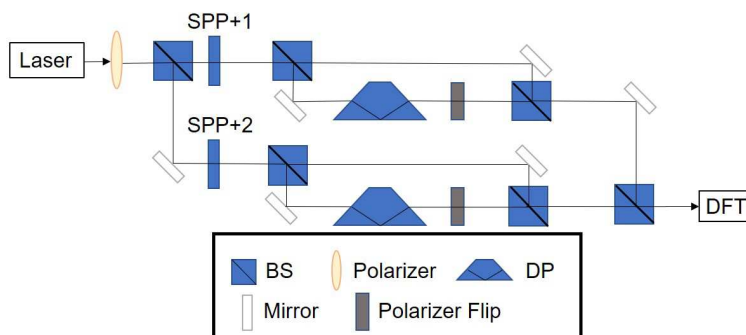


Figure 2. Optical path diagram of modular exponentiation in Shor's algorithm. A CW laser beam passes through the polarizer and SPPs to generate the OAM modes of Laguerre-Gaussian beams, which refer to different states in the algorithm. The DPs, polarizer flips, and BSs are used to execute the algorithm. BS indicates 50/50 beam splitters, SPP spiral phase plates, and DP Dove prisms.

The optical path setup for modular exponentiation is shown in Fig. 2. The light source is a CW laser such as HeNe laser [23], which is let pass through a horizontal polarizer and split into two equal intensity beams of the same horizontal polarization along two paths. These two paths are identical except for the spiral phase plates (SPP) which modulate identical beams into distinct OAM modes with  $l = +1$  and  $l = +2$ [27], giving rise to computational states  $|+1, H\rangle$  and  $|+2, H\rangle$ , respectively. Each of the beams are then passed through a beam splitter (BS), from which one branch goes through a Dove prism (DP) to invert the OAM sign ( $+1 \rightarrow -1$  or  $+2 \rightarrow -2$ ) [28] and a polarizer set to flip  $|H\rangle$  to  $|V\rangle$ , while the other branch remains unchanged. Eventually, the four branches of the two beams are recombined using three beam splitters, giving rise to the desired state after MEF according to Eq. (5).

## 2. Discrete Fourier Transform (DFT)

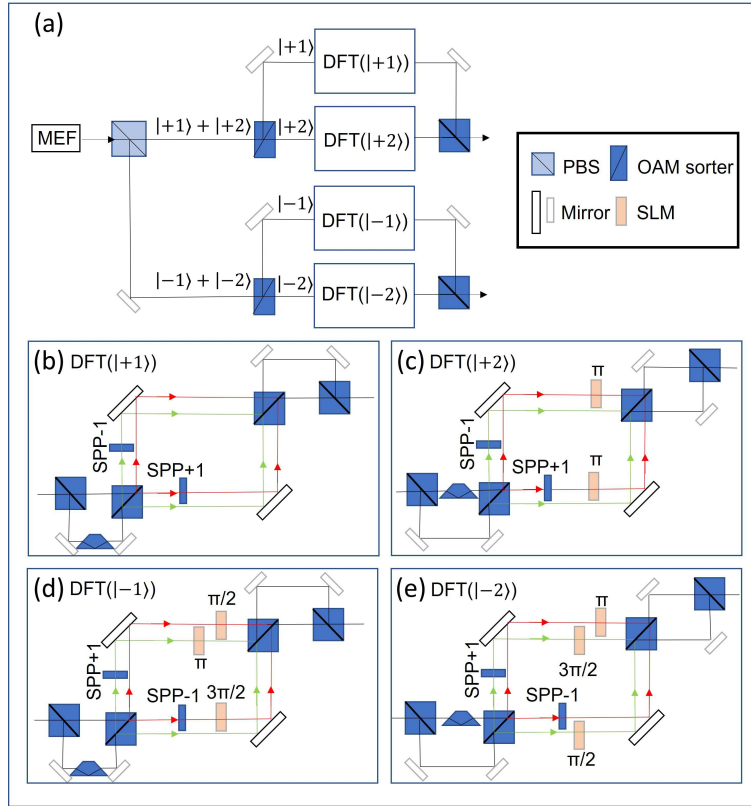


Figure 3. Optical path diagram of DFT in Shor's algorithm. The work register is measured to different polarization directions by a PBS. Each beam is sorted by an OAM sorter into two beams with different OAM and then emulates the DFT individually. Finally combining the beams and getting the output related to the order. SLM is phase-only spatial light modulator.

The optical path setup of DFT is illustrated in Fig. 3. The output of MEF is connected to the input of this step. As explained in the last section, the classical light path needs to achieve an effect analogous to quantum collapse to elicit beam states useful for computational purposes before feeding them into subsequent stages. To do this, the output beam from the MEF stage is split into two through a polarizer, allowing one to obtain the states of Eq. (6). Then, each polarized vortex beam is further split by an OAM sorter [29] into two, each carrying a particular OAM state. Considering all these four OAM states running in parallel, DFT effectively implements a  $4 \times 4$  matrix transformation on them, where the matrix entries represent complex phase coefficients of a Fourier transform.

Realizing these phases of this matrix to arrive at the resulting state of Eq. (9) relies on Sagnac interferometry. Each beam for a particular OAM state  $|j\rangle$  is first superposed with its inverse state  $| -j\rangle$  through beam splitters and a Dove prism, e.g.  $|+1\rangle \rightarrow |+1\rangle + |-1\rangle$ , before it enters its designated interferometer. Inside each interferometer, the SPPs generate the new OAM basis, e.g.  $|+1\rangle \rightarrow |+1\rangle + |+2\rangle$  and  $|-1\rangle \rightarrow |-1\rangle + |-2\rangle$ , whilst the SLMs generate corresponding phases along the state-designated paths. The beams are eventually combined using BS to output the computed state as in Eq. (9). This state then enters the final stage of interference fringe detection to obtain the information of multiplicative order.

#### IV. DETECTION OF RESULT STATES

The output beams from the DFT stage are LG beams comprising different OAM states with computational values. The last step of the setup is light paths that are responsible for telling what computational states are contained in these LG beams. To visually discern the computational states, we follow a proposal given in Ref. [25] to let the distinct OAM states interfere with each other, generating unique fringe patterns that are one-one corresponding to the quantum states. In other words, the desired multiplicative order is implied in a two-dimensional fringe image projected on a screen, as illustrated in Fig. 4.

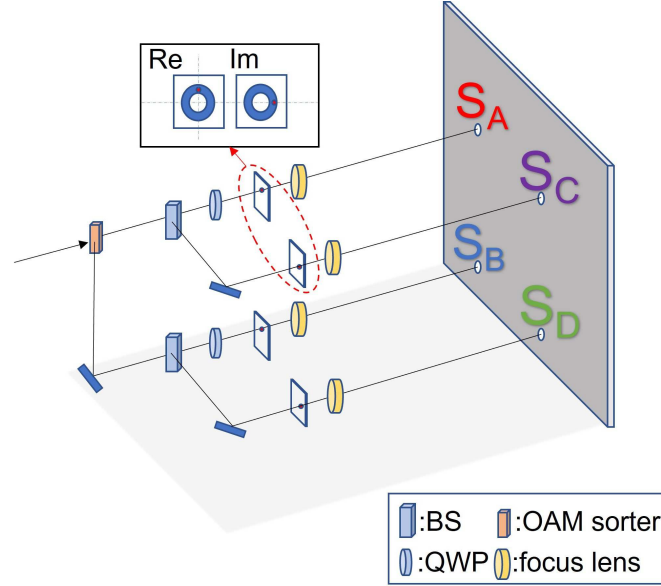


Figure 4. Optical path diagram of the detection method. The DFT output beam first goes through an OAM sorter to separate the beam into different OAM modes. Then two beams are decomposed into four beams by two BSs. By the orthogonal aperture diaphragms, the LG beams are separated into the real and imaginary components. Finally, refocused beams enter the four holes as the interference sources. The elements in the upper box represent the orthogonal aperture diaphragms; BS indicates beam splitter and QWP quarter-wave plate.

To implement the interference apparatus, the output from DFT is fed into an OAM sorter to obtain two beams with different  $l$  modes. Then along each beam path, we use a BS to further split it into two equal parts, constituting four beam paths. Two quarter-wave plates (QWP) are used to compensate for the phase shift introduced by BSs. One orthogonal aperture diaphragm is placed at each transmitted path to select two points from the real and imaginary components of each OAM state. For example, for the LG beam in Eq. 2, the intensity distribution is a helical doughnut with a phase dependence of  $\exp(-il\varphi)$ . The choice of real and imaginary parts depends on the azimuth  $\varphi$ , which is shown in the illustration of Fig. 4. Two points at the vertical and horizontal axis of the intensity distribution of two equal beams are chosen as the real and imaginary parts, respectively. Finally, the deflected beams from the holes are refocused, acting as the four sources  $S_A$ ,  $S_B$ ,  $S_C$  and  $S_D$  for the four-hole interference. For better interference effect, motorized translation stages (not drawn in the figure) can be used to synchronize the delays among paths.

We simulate the interference patterns by encoding the four light sources. A source laser wavelength of 632 nm, a hole to hole distance of 10  $\mu\text{m}$ , a hole to screen distance of 10 cm, and a screen area of 10  $\times$  10  $\text{cm}^2$  are assumed. Meanwhile, we set the  $z = 0, p = 0$  in Eq. (2) for the source beam for simplification. The interference fringe patterns are shown in Figs. 5 and 6.

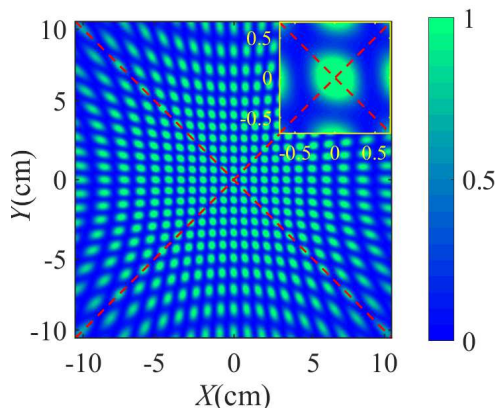


Figure 5. Interference patterns after DFT for state  $|+1\rangle+|+2\rangle$ .  $|+1\rangle$  and  $|+2\rangle$  means 0 and 2 respectively. Eliminating the impossible order 0, one gets the correct order  $r = 2$ .

The pattern in Fig 5 corresponds to the beam state of  $|+1\rangle+|+2\rangle$  at the DFT output, which is symmetric about the two diagonal axes. The central area is a bright spot. As shown in Ref. [25], the elliptical spot pattern has its major to minor axis ratio one-one corresponding to the coefficients of the eigenstates. Therefore, in a real experimental setup, the fringe patterns can be pre-generated as computer pixelated images, with which the projected interference image captured on, say, CCD sensor is compared. Since identifying bitmap images to compute the spot ratios are image recognition related, it does not incur extra computational complexity. Then, in the case demonstrated here, the two identified eigenstates are  $|+1\rangle$  and  $|+2\rangle$ , inferring a multiplicative order of 0 and 2, respectively. Since the order cannot be 0, one arrives at the correct order of  $r = 2$ .

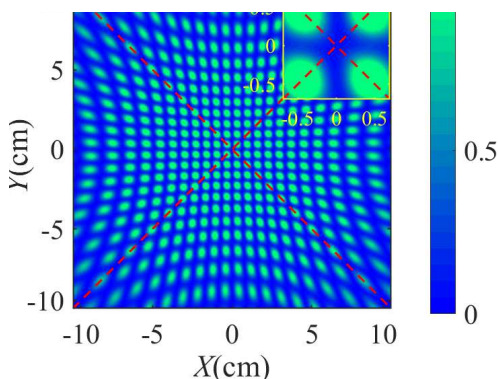


Figure 6. Interference patterns after DFT for state  $|+1\rangle-|+2\rangle$ , which also corresponds to the multiplicative order  $r = 2$ .

In the other case of  $|+1\rangle-|+2\rangle$ , the resulting fringe as shown in Fig. 6 is still symmetric about two diagonal axes though a dark area appears at the image center. The translational shift of the bright spot from the center to the neighboring locations on the diagonals reflects

the phase difference of the coefficients of  $|+1\rangle$  and  $|+2\rangle$ , i.e. changing from 0 for the  $|+1\rangle + |+2\rangle$  state to  $\pi$  for the  $|+1\rangle - |+2\rangle$  state. Since the spot still retains the same elliptical axis ratio, the identified magnitudes of the coefficients remain unchanged. It means that we also derive the states  $|+1\rangle$  and  $|+2\rangle$  as the final result from the fringe pattern, disregarding the phase difference, and arrive at the same correct order of 2.

## V. CONCLUSIONS AND DISCUSSIONS

We have demonstrated in principle that the quantum computational Shor's algorithm is in fact implementable using exclusively classical systems only. The classical entangled pair of OAM mode and polarization in LG beams are used as the control and the work registers, respectively. A detection method based on four-hole interference for the entangled states is demonstrated to obtain the multiplicative order  $r$ , which is equivalent to having found a factor once Euclid's classical gcd algorithm is applied. This order is uniquely determined by the two-dimensional fringe patterns.

Indeed the key quantum mechanical feature that Shor's algorithm takes advantage of is the formation of superposition states that imply quantum entanglement between states of number-theoretic value. The essence of entanglement here is the anomalous correlation that violates Bell's inequality [2]. It does not require the other aspect: states being nonlocal. Given its Bell parameter of correlation  $> 2$  [9], the classically generated entanglement fulfills the requirement of a locally executed algorithm. This explains why LG beams would work as the information carrier, which would otherwise be played by single-photon pairs, trapped ions, or superconducting qubits in the quantum regime. Compared to these quantum counterparts, the classical approach avoids the implementations of time-based quantum gates, eliminating the troublesome decoherence problem.

From a computational perspective, the classical approach admits a reduction of complexity similar to Shor's original formulation since both the classical and the quantum entangled states undergo identical modular exponentiation and Fourier transformation steps. But we note that the classical approach is trading space complexity with time complexity. Whereas the original QFT is implemented by a series of temporally ordered quantum gates, the DFT as shown in Fig. 3 is implemented by a collection of light path modules running in parallel, whose size scales with the integer  $N$  to be factored. Subsequently studies, therefore, will be devoted to the elimination of this disadvantage. Nevertheless, the work here extends the boundary of classical optics into quantum regime. Like other works on emulating quantum behavior with classical systems, it shows the line separating the quantum from the classical world is less well-defined than normally thought.

## ACKNOWLEDGMENTS

H.I. thanks the support by FDCT of Macau under Grant 0130/2019/A3 and by University of Macau under MYRG2018-00088-IAPME.

- 
- [1] A. Einstein, B. Podolsky, and N. Rosen, "Can Quantum-Mechanical Description of Physical Reality Be Considered Complete?" *Phys. Rev.* **47**(10), 777–780 (1935).
  - [2] J. S. Bell, "On the Einstein Podolsky Rosen paradox," *Physics Physique Fizika* **1**(3), 195–200 (1964).
  - [3] J. F. Clauser, M. A. Horne, A. Shimony, and R. A. Holt, "Proposed Experiment to Test Local Hidden-Variable Theories," *Phys. Rev. Lett.* **23**(15), 880–884 (1969).
  - [4] N. D. Mermin, "Extreme quantum entanglement in a superposition of macroscopically distinct states," *Phys. Rev. Lett.* **65**(15), 1838–1840 (1990).
  - [5] R. Horodecki, P. Horodecki, M. Horodecki, and K. Horodecki, "Quantum entanglement," *Rev. Mod. Phys.* **81**(2), 865–942 (2009).

- [6] R. J. C. Spreeuw, “A Classical Analogy of Entanglement,” *Found. Phys.* **28**(3), 361–374 (1998).
- [7] X.-F. Qian and J. H. Eberly, “Entanglement and classical polarization states,” *Opt. Lett.* **36**(20), 4110–4112 (2011).
- [8] A. Aiello, F. Töppel, C. Marquardt, E. Giacobino, and G. Leuchs, “Quantum-like nonseparable structures in optical beams,” *New J. Phys.* **17**(4), 043024 (2015).
- [9] X.-F. Qian, B. Little, J. C. Howell, and J. H. Eberly, “Shifting the quantum-classical boundary: theory and experiment for statistically classical optical fields,” *Optica* **2**(7), 611–615 (2015).
- [10] X. Song, Y. Sun, P. Li, H. Qin, and X. Zhang, “Bell’s measure and implementing quantum Fourier transform with orbital angular momentum of classical light,” *Sci. Rep.* **5**(1), 14113 (2015).
- [11] P. W. Shor, “Algorithms for quantum computation: discrete logarithms and factoring,” in *Proceedings 35th Annual Symposium on Foundations of Computer Science* (1994), pp. 124–134.
- [12] P. Shor, “Polynomial-Time Algorithms for Prime Factorization and Discrete Logarithms on a Quantum Computer”, *SIAM J. Comput.* **26**, 1484 (1997).
- [13] E. Lucero, R. Barends, Y. Chen, J. Kelly, M. Mariantoni, A. Megrant, P. O’Malley, D. Sank, A. Vainsencher, J. Wenner, T. White, Y. Yin, A. N. Cleland, and J. M. Martinis, “Computing prime factors with a Josephson phase qubit quantum processor,” *Nat. Phys.* **8**(10), 719–723 (2012).
- [14] L. M. K. Vandersypen, M. Steffen, G. Breyta, C. S. Yannoni, M. H. Sherwood, and I. L. Chuang, “Experimental realization of Shor’s quantum factoring algorithm using nuclear magnetic resonance,” *Nature* **414**(6866), 883–887 (2001).
- [15] C.-Y. Lu, D. E. Browne, T. Yang, and J.-W. Pan, “Demonstration of a Compiled Version of Shor’s Quantum Factoring Algorithm Using Photonic Qubits,” *Phys. Rev. Lett.* **99**(25), 250504 (2007).
- [16] A. Politi, J. C. F. Matthews, and J. L. O’Brien, “Shor’s Quantum Factoring Algorithm on a Photonic Chip,” *Science* **325**(5945), 1221–1221 (2009).
- [17] E. Martín-López, A. Laing, T. Lawson, R. Alvarez, X.-Q. Zhou, and J. L. O’Brien, “Experimental Realization of Shor’s Quantum Factoring Algorithm Using Qubit Recycling”, *Nat. Photo.* **6**, 11 (2012).
- [18] A. Forbes, A. Aiello, and B. Ndagano, “Chapter Three - Classically Entangled Light,” in *Progress in Optics*, T. D. Visser, ed. (Elsevier, 2019), 64, pp. 99–153.
- [19] T. D. Ladd, F. Jelezko, R. Laflamme, Y. Nakamura, C. Monroe, and J. L. O’Brien, “Quantum computers,” *Nature* **464**(7285), 45–53 (2010).
- [20] F. Töppel, A. Aiello, C. Marquardt, E. Giacobino, and G. Leuchs, “Classical entanglement in polarization metrology,” *New J. Phys.* **16**(7), 073019 (2014).
- [21] R. J. C. Spreeuw, “Classical wave-optics analogy of quantum-information processing,” *Phys. Rev. A* **63**(6), 062302 (2001).
- [22] D. Deutsch and R. Penrose, “Quantum theory, the Church–Turing principle and the universal quantum computer,” *Proceedings of the Royal Society of London. A. Mathematical and Physical Sciences* **400**(1818), 97–117 (1985).
- [23] B. Perez-Garcia, J. Francis, M. McLaren, R. I. Hernandez-Aranda, A. Forbes, and T. Konrad, “Quantum computation with classical light: The Deutsch Algorithm,” *Phys. Lett. A* **379**(28), 1675–1680 (2015).
- [24] S. K. Goyal, F. S. Roux, A. Forbes, and T. Konrad, “Implementing Quantum Walks Using Orbital Angular Momentum of Classical Light,” *Phys. Rev. Lett.* **110**(26), 263602 (2013).
- [25] Z. You, Y. Wang, Z. Tang, and H. Ian, “Measurement of Classical Entanglement Using Interference Fringes,” *J. Opt. Soc. Am. B* **38**, 1798 (2021).
- [26] L. Allen, M. W. Beijersbergen, R. J. C. Spreeuw, and J. P. Woerdman, “Orbital angular momentum of light and the transformation of Laguerre-Gaussian laser modes,” *Phys. Rev. A* **45**(11), 8185–8189 (1992).
- [27] M. W. Beijersbergen, R. P. C. Coerwinkel, M. Kristensen, and J. P. Woerdman, “Helical-wavefront laser beams produced with a spiral phase plate,” *Opt. Commun.* **112**(5), 321–327 (1994).
- [28] N. González, G. Molina-Terriza, and J. P. Torres, “How a Dove prism transforms the orbital angular momentum of a light beam,” *Opt. Express*, **14**(20), 9093–9102 (2006).
- [29] J. Leach, M. J. Padgett, S. M. Barnett, S. Franke-Arnold, and J. Courtial, “Measuring the Orbital Angular Momentum of a Single Photon,” *Phys. Rev. Lett.* **88**(25), 257901 (2002).